Communication

A Novel Systematic Design of High-Aperture-Efficiency 2D Beam-Scanning Liquid-Crystal Embedded Reflectarray Antenna for 6G FR3 and Radar Applications

Hogyeom Kim, Jongyeong Kim, and Jungsuek Oh

***Abstract*— This communication presents a novel systematic design of a high-aperture-efficiency and 2-D beam-scanning nematic liquid-crystal (LC)-based reflectarray (LCRA) that operates in the sixth-generation (6G) midband (7–24 GHz). Despite a 260° phase range, the maximum aperture efficiency is 35.8% at an aperture dimension (F/D) ratio of 0.58, the highest aperture efficiency at the lowest F/D ratio among LCRAs designed to operate on the mmWave band. The proposed LC-based reflectarray unit cell (LC-RUC) has significantly low reflection loss compared to other LC-RUCs. Also, the bias topology of the proposed LC-RUC makes the LCRA capable of 2-D beam scanning. The beam-scanning range of the proposed LCRA is ±50° on the *xoz* plane and 0°–65° in the *yoz* plane at 9.55 GHz. A 2 × 2 patch array antenna is designed as the feed antenna to achieve a small F/D ratio system and ease of optimization. When designing the feed antenna, the number of elements or the element spacing is considered to achieve high feed efficiency. In addition, the fabricated planar feed antenna can be easily integrated with a 3-D printed jig in which the focal length can be adjusted for optimization. The lowest side lobe level (SLL) of the proposed LCRA is −15.5 dB.**

***Index Terms*— Liquid crystals (LCs), radar, reconfigurable unit cell, reflectarray antennas, sixth-generation (6G) midband.**

I. Introduction

Recently, sixth-generation (6G) standardization and numerous corresponding antennas have been actively reported and studied [1], [2], [3], [4]. While the potential 6G frequency band is being considered to be sub-THz [5], [6], midband within the 7–24 GHz is also regarded as a future 6G band [7]. Implemented tasks, such as antenna design, manufacturing, and measurement in that band, are more modest than those of the sub-THz. In the midband, many types of planar patch, transmit, and reflectarray antennas are employed in the radar application [8], [9], [10], and this study addresses a reflectarray antenna.

A reflectarray antenna consists of 2-D periodic patterns printed onto a grounded substrate. This structure has several advantages, including ease of fabrication, planarity, and low cost. Recently, numerous studies of electronically controllable reflectarray antennas, which operate on the mmWave band, have been conducted. Examples include the pin diode, varactor diode, and liquid crystal (LC) types [11], [12], [13], [14]. LC-based reflectarray (LCRA) antennas radiate scattered waves toward the desired direction as the permittivity of the embedded LC changes. LCRA antennas offer several advantages, including continuous phase control and low heat [15], [16], [17]. Also, the LCRA can be operated on various frequency bands ranging from the X-band to the THz band [18], [19]. Compared to other active components, such as a pin diode and a varactor diode, the loss tangent of the LC decreases as the frequency increases [20], [21].

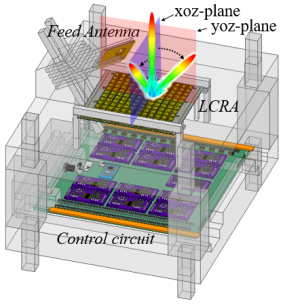

Fig. 1. Schematic of the proposed LCRA.

However, an LCRA with an aperture efficiency exceeding 30% has not yet been reported due to fabrication errors, a lack of optimization, and high reflection loss of the unit cells. There are several LCRA structures published in the prior works. In one study [13], multiresonant cells resembling a dipole array are employed for a broadband reflectarray antenna. The unit cell has a high reflection loss, and the bias layout limits the beamforming along one dimension, resulting in low aperture efficiency. In another study [20], employing a delay line near the LC layer introduces broadband characteristics, and such an antenna is capable of 2-D beam scanning. Although the aforementioned LCRA structure [20] was the first to be capable of 2-D-beam scanning on the mmWave band, the aperture efficiency is low due to the high reflection loss (a maximum reflection loss is 7 dB) of the unit cell. In order to achieve high aperture efficiency, the unit cell and feed efficiency are the key factors.

Recently, Kim *et al.* [22] reported a low-loss LC-based reflectarray unit cell (LC-RUC) for use on the X-band. Generally, the reflection loss of an LC cell can be reduced by increasing the LC thickness. However, when the LC thickness increases, the response time of the LC also increases. In the low-loss LC-RUC, a metallic patch is added onto the superstrate, resulting in a change of the input impedance. Then, the reflection loss decreases as the superstrate increases without increasing the LC thickness. Also, the optimization of the feed efficiency is described in this communication. Fig. 1 shows a schematic of the proposed LCRA composed of the feed antenna, the LCRA, and the control circuit. The proposed LCRA consists of a 12 × 12 LC-RUC, where each cell is based on a low-reflection-loss design [22]. The significant low reflection loss enables achieving

Manuscript received 22 December 2021; revised 5 July 2022; accepted 29 July 2022. Date of publication 30 September 2022; date of current version 17 November 2022. This work was supported by the Grant-in-Aid of Hanwha Systems Based on the Challenging Future Defense Technology Research and Development Program of the Agency for Defense Development in 2019 under Grant 9127786. *(Corresponding author: Jungsuek Oh.)*

Hogyeom Kim and Jungsuek Oh are with the Institute of New Media and Communication (INMC) and the Department of Electrical and Computer Engineering, Seoul National University, Seoul 08826, South Korea (e-mail: ghrua2424@snu.ac.kr; jungsuek@snu.ac.kr).

Jongyeong Kim is with the Special Radar Team, Hanwha Corp Defense Division, Jung-gu 04541, South Korea (e-mail: icejong41@hanwha.com).

Color versions of one or more figures in this communication are available at https://doi.org/10.1109/TAP.2022.3209178.

Digital Object Identifier 10.1109/TAP.2022.3209178

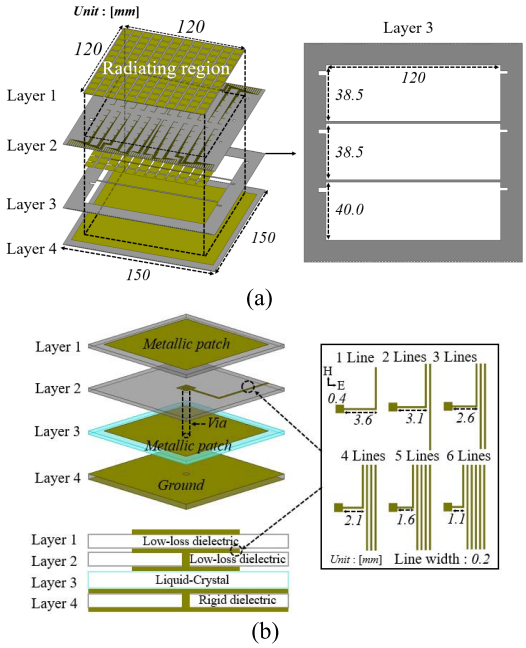

Fig. 2. Exploded view of (a) proposed LCRA and (b) LC-RUC.

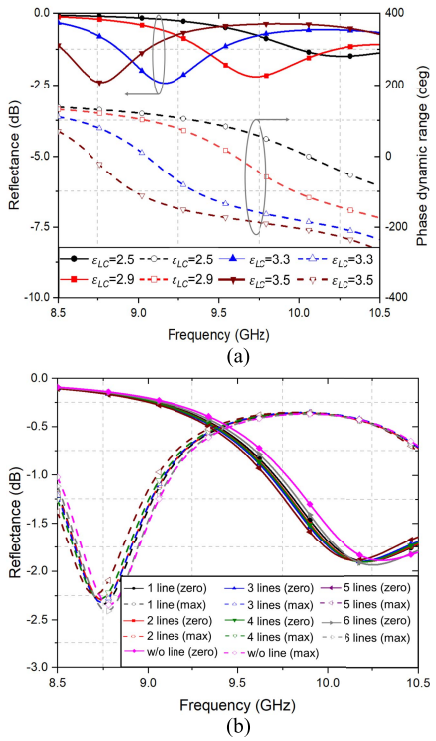

Fig. 3. Frequency responses of (a) magnitude and phase dynamic range versus permittivity of the LC-RUC and (b) magnitude responses versus the number of lines [solid lines: zero bias ($\varepsilon_{\perp}$) and dashed lines: maximum bias state ($\varepsilon_{\parallel}$)].

high aperture efficiency despite a lack of phase shift range due to the short electrical length. A 2 × 2 patch array antenna is chosen as the feed antenna to achieve a small ratio of focal length to aperture dimension (F/D) ratio system owing to its wide beam-width. The proposed LCRA is capable of 2-D beamforming, achieving an aperture efficiency of more than 35% with a side lobe level (SLL) of −15.5 dB.

This study is organized as follows. In Section II-A, the design of the proposed LCRA and LC-RUC is introduced. Also, the frequency responses of the LC-RUC are discussed. In Section II-B, the optimum focal length of the feed antenna and the corresponding feed efficiency are calculated in a full-wave EM simulation. In Section III-A, the measurement setup and phase extraction are introduced for 2-D beam scanning. In Section III-B, the measurement results are presented and discussed. Finally, the study is concluded in Section IV.

II. LCRA Design

A. Design of the Proposed LCRA

The geometrical details of the proposed LCRA are shown in Fig. 2. The radiating region is 120 × 120 mm, and the periodicity of the proposed LC-RUC is 10 mm. The additional area, except for the radiating region, will be covered by the absorber. On the second layer, the bias lines are connected to the control circuit through metallic vias on the edges of the layers. The third layer is divided into three compartments in order to create a cavity to accommodate the LC. The metallic surface on the top of the fourth layer acts as radio frequency (RF) and dc ground at the same time. Also, in order to easily connect the dc ground to the outer control circuit, the metallic surface is placed at the bottom side and connected to the surface on the top side through the via. Fig. 2(b) shows an exploded view of the LC-RUC. A metallic patch on the first layer is introduced to achieve low reflection loss. The metallic patch affects the actual input impedance, enabling a reduction of the reflection loss by increasing the thickness of the first layer or the second layer. Six types of bias lines are employed to ensure dc bias in the second layer. Each bias line is connected to the metallic patch on the third layer in order to excite the E-field toward the LC layer. The third layer consists of the LC, and the relative permittivity of the LC has a complex value ($\varepsilon'_{LC} - j\varepsilon''_{LC}$) due to its loss feature. Based on its datasheet, the tunable range of the dielectric constant of the *LC* used in this study is expected to be 2.5–3.5 (from $\varepsilon_{\perp}$ to $\varepsilon_{\parallel}$) [23], and the corresponding loss tangent decreases from 0.012 to 0.0064. The dimensions of the metallic patches are 8.4 × 8.4 mm and the width and length of each bias line are shown in Fig. 2(b). The Taconic TLY-5 and FR4 are chosen as the low-loss dielectric and the rigid dielectric, respectively. The dielectric constant and the loss tangent of the TLY-5 are 2.2 and 0.0009, respectively, and those of the FR4 are 4.4 and 0.02, respectively.

Fig. 3(a) shows the frequency responses of the magnitude and the phase dynamic range versus the permittivity of the proposed LC-RUC. The simulation results were obtained from a Floquet simulation in Ansys HFSS. In the simulation, the permittivity of the LC is considered as an effective scalar value [20], [24], [25].

Solid lines and dashed lines represent the magnitude and phase responses, respectively. The maximum reflection loss and the dynamic phase shift range at the 9.55 GHz target frequency are 2.3 dB and 260°, respectively. The reflection loss of 2.3 dB is significantly low compared to those of other LC-RUCs that run on the X-band [18], [30]. The proposed LCRA can achieve high aperture efficiency even with a phase shift range of 260° compared to other published LCRA. Fig. 3(b) shows an effect of the bias layer. The reflection magnitude responses in the zero and maximum bias states of the LC versus the number of lines are shown in Fig. 3(b). The number of the bias lines has little impact on the unit cell.

B. Feed Antenna Design and Configuration

In this communication, to achieve a small F/D ratio system, a 2 × 2 patch array is utilized as the feed antenna because it has a wider 3 dB beamwidth and smaller size than the horn antenna. There are several advantages when employing this type of patch array.

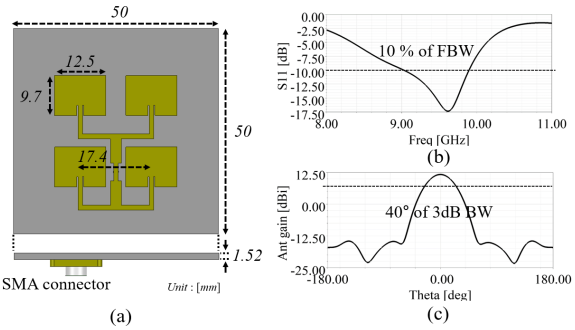

Fig. 4. (a) Designed 2 × 2 patch array antenna. (b) Impedance bandwidth. (c) 3 dB beamwidth.

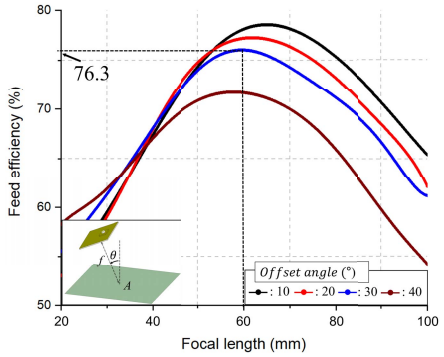

Fig. 5. Calculated feed efficiency as a function of the focal length.

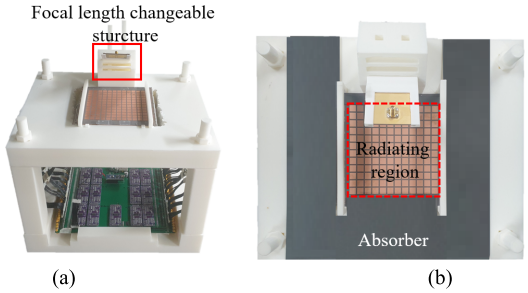

Fig. 6. (a) Oblique view and (b) top view of the fabricated proposed LCRA sample.

First, the 3 dB beamwidth can be adjusted easily by increasing the number of elements or the element spacing. The 3 dB beamwidth is an important factor in the design of the high-efficiency reflectarray. Second, the fabrication cost can be reduced by the PCB-based process compared to that of a horn antenna. Finally, a planar antenna can easily be integrated with the 3-D printed jig, enabling optimization of the LCRA.

Fig. 4 shows the designed feed antenna, impedance bandwidth, and the 3 dB beamwidth. The TLY-5 is employed to design the feed antenna. Here, a fractional bandwidth (FBW) of 10% and a 3 dB beamwidth of 40° are obtained. The optimum focal length should be selected when the feed efficiency (taper × spillover efficiencies, without consideration of radiation efficiency) reaches its maximum value for high efficiency.

The taper and spillover can be calculated as shown in the following. First, the symmetric feed-power pattern can be modeled as expressed in the following equation:

$$G_{feed} \propto \cos^{q}\theta. \tag{1}$$

If the antenna's 3 dB beamwidth narrows, the value of q increases. By employing this equation, the taper and spillover efficiency are calculated as correspondingly expressed in the following equations [26]:

$$\eta_{taper} = \frac{2q}{\tan^2\theta_{sub}} \frac{1-\cos^{(q/2)-1}\theta_{sub}}{\left(\frac{q}{2}-1\right)^2\left(1-\cos^{q}\theta_{sub}\right)} \tag{2}$$

$$\eta_{spillover} = 1-\cos^{q+1}\theta_{sub}. \tag{3}$$

Here, θ_{sub} is the subtended angle, defined via the following equation:

$$\theta_{sub} = \tan^{-1}\frac{A}{2f}. \tag{4}$$

In addition, A and f represent the aperture dimension and focal length, respectively. This method is very fast in terms of time because the calculation is processed in MATLAB. However, when considering the sidelobe or offset feed angle, this method lacks accuracy. Second, by employing a full-wave simulator such as the Ansys HFSS, the feed efficiency and optimum offset feed angle can be calculated. The feed efficiency is obtained by multiplying (5) by (6) [27]

$$\eta_{taper} = \frac{1}{A}\frac{\left|\iint_A I dA\right|^2}{\iint_A |I|^2 dA} \tag{5}$$

$$\eta_{spillover} = \frac{\iint_A \vec{S}\cdot d\vec{A}}{P_{rad}}. \tag{6}$$

Here, I, S, and P_{rad} are the field intensity, Poynting vector, and radiated power from the feed antenna, respectively. This method is more accurate than the first method but is time-consuming as well. Therefore, the approximate focal length was calculated with the first method, after which fine-tuning optimization was done with the second method. Fig. 5 shows the calculated results of the feed efficiency as a function of the focal length at the target frequency. An offset angle of 30° and a focal length of 60 mm were selected as the candidate value for the feed antenna configuration. The corresponding feed efficiency is 76.3%.

III. Measurement Results and Discussion

A. Measurement Setup and Phase Extraction

Fig. 6 shows a fabricated example of the proposed LCRA sample integrated with the feed antenna and control circuit by the 3-D printed jig. The focal length can be adjusted from 6 to 9 cm in the 3-D-printed jig. In Fig. 6(b), the absorber is placed on the jig, covering the additional region. Therefore, the incident and scattered waves occur at the radiating region.

The measurement setup is shown in Fig. 7. The distance between the reflectarray and the receiver is set to 1.5 m. The control circuit is connected to a laptop. The control circuit can support voltage levels from 0 to 30 V in steps of 0.1 V. When the desired voltage levels are typed into the software tool, the tool orders the control circuit to provide the corresponding voltage level, resulting in bias in each LC in the RUC. In order to form the beam, bias voltage sets for the desired phase shift should be obtained. Also, due to the anisotropy and inhomogeneity in the direction of the bias field for intermediate states in the cells, the bias voltage for the desired phase shift can only be determined after measuring the phase [28]. The desired bias voltage levels can be obtained via the following steps.

1) Apply the same voltage to all unit cells.
2) Allow the phase of S_{21} in the vector network analyzer (VNA) to change as the bias voltage level changes.

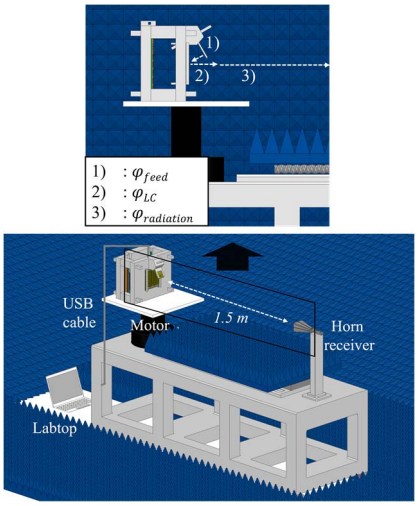

Fig. 7. Measurement setup.

TABLE I

VOLTAGE LEVELS FOR THE DESIRED PHASE SHIFT AND THE MAGNITUDE FLUCTUATION

Voltage level (V)	Phase Δ (°)	Magnitude Δ (dB)
0	0	0
1.6	-40	-1.6
2.0	-90	-1.8
2.3	-130	-2.0
5.1	-180	-1.4
6.5	-230	-0.8
11.0	-260	+0.2

Δ represents the difference between the no-bias state and a certain bias state. The maximum voltage level is 11.0 V.

3) Obtain the bias voltage level for the desired phase shift from the following equation:

$$\varphi_{S_{21}} = \varphi_{feed} + \varphi_{LC} + \varphi_{radiation}. \tag{7}$$

As shown in Fig. 7, φ_{feed} refers to the phase shift of the radiated waves from the feed antenna to the reflectarray, and φ_{LC} represents the reflection phase shift resulting from the change of the LC. In addition, $\varphi_{radiation}$ refers to the phase shift of the radiated waves from the reflectarray to the receiver. If all unit cells are biased with the same voltage level, only φ_{LC} will change. Thus, the desired phase shift can be obtained. Table I shows the obtained voltage levels for the desired phase shift and the corresponding magnitude fluctuation.

B. Discussion of Measured Results

This section discusses the measured results for the proposed LCRA. The measurements were implemented in an anechoic chamber, and the measurement of the S-parameter was obtained by a VNA, the MS4647A type from Anritsu. The measured results were obtained by applying various voltage sets according to the reference phase [27].

In Fig. 8, the simulated and measured results at 9.55 GHz are shown. The final focal length is 7 cm. Although the calculated focal length is 6 cm, the fabricated sample shows a maximum gain at 7 cm. On the *xoz* plane, the simulated gain and measured gain are 15.6–18.4 dBi and 14.7–17.1 dBi, respectively. Also, the simulated and measured SLLs are −10.2 to −17.4 dB and −8.2 to −15.5 dB,

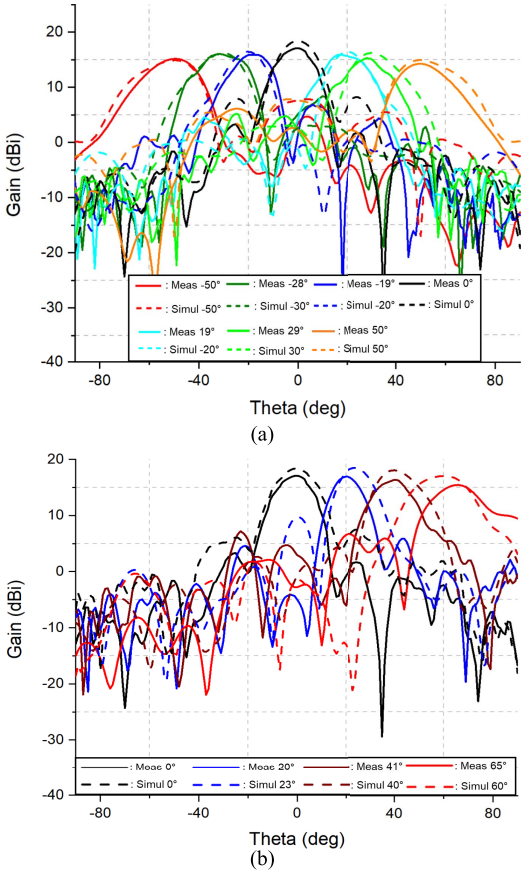

Fig. 8. Simulated and measured beam pattern results at 9.55 GHz on (a) *xoz* plane and (b) *yoz* plane.

TABLE II

PERFORMANCE COMPARISON OF LCRA ANTENNAS

Feature	Ref. [13]	Ref. [30]	Ref. [31]	Ref. [20]	This work
Frequency [GHz]	100	9.4	24	24	9.55
Max. AE [%]	18.5	-	5.8	23.1	35.8
Max. RL [dB]	7	18	2.5	7	2.3
SLL [dB]	-13.0	-	-	-	-15.5
Scanning capability	1D	1D	1D	2D	2D
Scanning range [°]	55	40	20	90	100
F/D	-	1.07	-	1.0	0.58

※AE: aperture efficiency, RL: reflection loss

respectively. The maximum gain occurs at 0°. There is a lower SLL in measurements than in simulation because of the low magnitude fluctuation. The error range between the simulated and measured gains is 0.2–1.3 dB. The cause of the error is the coupling among biased cells and fabrication error. The scanning range is −50° to 50°. However, the scanning range on the *yoz* plane is 0°–65° due to the blockage of the feed antenna. The simulated gain and the measured gain on the *yoz* plane are 16.0–18.4 dBi and 15.4–17.1 dBi, respectively. The simulated and measured SLLs are −8.8 to −14.2 dB and −8.7 to −13.8 dB, respectively. Although the maximum gain

occurs at 0°, the maximum aperture efficiency is at 65° because the effective aperture decreases as the scan angle increases [19]. Therefore, the aperture efficiency at 65° on the *yoz* plane is 35.8%. The 1 dB gain bandwidth is 9.05–9.95 GHz over the entire beam coverage. Table II shows a performance comparison of the LCRA. The proposed design has higher aperture efficiency and a wider beam-scanning range than other designs with a short focal length. The high aperture efficiency can be achieved with significantly low reflection loss, 2-D beam-forming capability, and optimization of the feed antenna.

IV. Conclusion

A novel systematic design of a 2-D beam-scanning and high-aperture-efficiency LCRA is introduced in this communication. The reported aperture efficiency of the LCRA proposed here is 35.8% at 9.55 GHz, the highest efficiency among LCRAs that operate on the mmWave, even given its low F/D ratio. Despite a lack of phase shift range, significant low reflection loss enables achieving high aperture efficiency. Also, the proposed design can steer the beam along two axes. The scanning range is ±50° on the *xoz* plane and 0°–65° on the *yoz* plane. Furthermore, a 2 × 2 patch array antenna is selected as the feed antenna to achieve a short F/D ratio system due to its wide beamwidth and ease of optimization. The proposed LCRA will be promising when designing high-efficiency 2-D beam-scanning LCRAs in the 6G midband.

References

[1] H. Tataria, M. Shafi, A. F. Molisch, M. Dohler, H. Sjöland, and F. Tufvesson, "6G wireless systems: Vision, requirements, challenges, insights, and opportunities," *Proc. IEEE*, vol. 109, no. 7, pp. 1166–1199, Jul. 2021.

[2] *6G: The Next Hyper-Connected Experience for All*, Samsung, Suwon-Si, South Korea, Jul. 2020.

[3] Z. Zhang *et al.*, "6G wireless networks: Vision, requirements, architecture, and key technologies," *IEEE Veh. Technol. Mag.*, vol. 14, no. 3, pp. 28–41, Sep. 2019.

[4] I. Yoon, S. Oh, and J. Oh, "Affordable thin lens usign signle polarized disparate filter arrays for beyond 5G toward 6G," *Sensors*, vol. 10, no. 18, Sep. 2019.

[5] J. Lee, H. Kim, and J. Oh, "Large-aperture metamaterial lens antenna for multi-layer MIMO transmission for 6G," *IEEE Access*, vol. 10, pp. 20486–20495, 2022.

[6] H. H. Bae, T. H. Jang, H. Y. Kim, and C. S. Park, "Broadband 120 GHz L-probe differential feed dual-polarized patch antenna with soft surface," *IEEE Trans. Antennas Propag.*, vol. 69, no. 10, pp. 6185–6195, Oct. 2021.

[7] K. Eun-Jin, "Samsung unveils 6G spectrum white paper and 6G research findings," BusinessKorea, Seoul, South Korea, May 2022.

[8] Y.-S. Yeoh and K.-S. Min, "Characteristics of 6×26 slotted waveguide array antenna for wave monitoring radar system," *J. Electromagn. Eng. Sci.*, vol. 21, no. 5, pp. 439–447, Nov. 2021.

[9] L. Di Palma, A. Clemente, L. Dussopt, R. Sauleau, P. Potier, and P. Pouliguen, "Radiation pattern synthesis for monopulse radar applications with a reconfigurable transmitarray antenna," *IEEE Trans. Antennas Propag.*, vol. 64, no. 9, pp. 4148–4154, Sep. 2016.

[10] S. Costanzo, F. Venneri, A. Raffo, G. Di Massa, and P. Corsonello, "Radial-shaped single varactor-tuned phasing line for active reflectarrays," *IEEE Trans. Antennas Propag.*, vol. 64, no. 7, pp. 3254–3259, Jul. 2016.

[11] E. Carrasco, M. Barba, and J. A. Encinar, "X-band reflectarray antenna with switching-beam using PIN diodes and gathered elements," *IEEE Trans. Antennas Propag.*, vol. 60, no. 12, pp. 5700–5708, Dec. 2012.

[12] F. Venneri, S. Costanzo, and G. Di Massa, "Design and validation of a reconfigurable single varactor-tuned reflectarray," *IEEE Trans. Antennas Propag.*, vol. 61, no. 2, pp. 635–645, Feb. 2013.

[13] G. Perez-Palomino *et al.*, "Design and demonstration of an electronically scanned reflectarray antenna at 100 GHz using multiresonant cells based on liquid crystals," *IEEE Trans. Antennas Propag.*, vol. 63, no. 8, pp. 3722–3727, Aug. 2015.

[14] B. Rana, I. Lee, and I. Hong, "Experimental characterization of 2×2 electronically reconfigurable 1 bit unit cells for a beamforming transmitarray at X band," *J. Electromagn. Eng. Sci.*, vol. 21, no. 2, pp. 153–160, Apr. 2021.

[15] A. Manabe, "Liquid crystals for microwave applications," in *Proc. 7th Eur. Conf. Antennas Propag. (EuCAP)*, Apr. 2013, pp. 1973–1974.

[16] W. Hu *et al.*, "Design and measurement of reconfigurable millimeter wave reflectarray cells with nematic liquid crystal," *IEEE Trans. Antennas Propag.*, vol. 56, no. 10, pp. 3112–3117, Oct. 2008.

[17] G. Perez-Palomino *et al.*, "Wideband unit-cell based on liquid crystals for reconfigurable reflectarray antennas in F-band," in *Proc. IEEE Int. Symp. Antennas Propag.*, Jul. 2012, pp. 1–2.

[18] M. Y. Ismail, R. Cahill, M. Amin, A. F. M. Zain, and M. K. Amin, "Phase range analysis of patch antenna reflectarray based on nematic liquid crystal substrate with dynamic RCS variation," in *Proc. Asia–Pacific Microw. Conf.*, Dec. 2007, pp. 1–4.

[19] J. Yang, P. Wang, S. Sun, Y. Li, Z. Yin, and G. Deng, "A novel electronically controlled two-dimensional terahertz beam-scanning reflectarray antenna based on liquid crystals," *Frontiers Phys.*, vol. 8, Oct. 2020, Art. no. 576045.

[20] X. Li *et al.*, "Broadband electronically scanned reflectarray antenna with liquid crystals," *IEEE Antennas Wireless Propag. Lett.*, vol. 20, no. 3, pp. 396–400, Mar. 2021.

[21] G. Perez-Palomino *et al.*, "Design and experimental validation of liquid crystal-based reconfigurable reflectarray elements with improved bandwidth in F-band," *IEEE Trans. Antennas Propag.*, vol. 61, no. 4, pp. 1704–1713, Apr. 2013.

[22] H. Kim, J. Kim, and J. Oh, "Liquid-crystal-based X-band reactively loaded reflectarray unit cell to reduce reflection loss," *IEEE Antennas Wireless Propag. Lett.*, vol. 20, no. 10, pp. 1898–1902, Oct. 2021.

[23] J. Kim and J. Oh, "Liquid-crystal-embedded aperture-coupled microstrip antenna for 5G applications," *IEEE Antennas Wireless Propag. Lett.*, vol. 19, no. 11, pp. 1958–1962, Nov. 2020.

[24] J. Yang *et al.*, "Fully electronically phase modulation of millimeter-wave via comb electrodes and liquid crystal," *IEEE Antennas Wireless Propag. Lett.*, vol. 20, no. 3, pp. 342–345, Mar. 2021.

[25] S. Bildik, S. Dieter, C. Fritzsch, W. Menzel, and R. Jakoby, "Reconfigurable folded reflectarray antenna based upon liquid crystal technology," *IEEE Trans. Antennas Propag.*, vol. 63, no. 1, pp. 122–132, Jan. 2015.

[26] D. M. Pozar, S. D. Targonski, and H. D. Syrigos, "Design of millimeter wave microstrip reflectarrays," *IEEE Trans. Antennas Propag.*, vol. 45, no. 2, pp. 287–296, Feb. 1997.

[27] A. Z. Elsherbeni, P. Nayeri, and F. Yang, *Reflectarray Antennas: Theory, Designs, and Applications*. Hoboken, NJ, USA: Wiley, 2018.

[28] G. Perez-Palomino *et al.*, "Accurate and efficient modeling to calculate the voltage dependence of liquid crystal-based reflectarray cells," *IEEE Trans. Antennas Propag.*, vol. 62, no. 5, pp. 2659–2668, May 2014.

[29] P. Hannan, "The element-gain paradox for a phased-array antenna," *IEEE Trans. Antennas Propag.*, vol. AP-12, no. 4, pp. 423–433, Jul. 1964.

[30] W. Hu *et al.*, "Liquid-crystal-based reflectarray antenna with electronically switchable monopulse patterns," *Electron. Lett.*, vol. 43, no. 14, pp. 744–745, 2007.

[31] W. Zhang, Y. Li, and Z. Zhang, "A reconfigurable reflectarray antenna with an 8 μm-thick layer of liquid crystal," *IEEE Trans. Antennas Propag.*, vol. 70, no. 4, pp. 2770–2778, Apr. 2021.